X-ray binaries in the Milky Way and other galaxies

Hans-Jakob Grimm[1] ⋆, Marat Gilfanov[2,3] and Rashid Sunyaev[2,3]

[1] Center for Astrophysics, 60 Garden Street, MS-29, Cambridge 02138, USA
[2] Max-Planck-Institut für Astrophysik Karl-Schwarzschild-Str. 1, 85741 Garching, Germany
[3] Space Research Institute of Russian Academy of Sciences, Profsoyuznaya 84/32, 117810 Moscow, Russia

Abstract We performed a study of the X-ray binary population in the Milky Way. The results of this study, spatial distribution and in particular luminosity function, can be used for comparison with the X-ray binary populations of other galaxies. In the second part we give an example by investigating the connection between the star formation rate and the high mass X-ray binary population in galaxies observed by CHANDRA.

Key words: X-rays: binaries – Galaxies: Milky Way – Luminosity function

1 INTRODUCTION

In the absence of a bright AGN, the X-ray emission of a galaxy is known to be dominated by the collective emission of its X-ray binary populations (see e.g. Fabbiano (1994)). X-ray binaries, conventionally divided into low and high mass X-ray binaries, consist of a neutron star (NS) or a black hole (BH) accreting from a normal companion star. To form a NS or BH the initial mass of the progenitor star must exceed $\sim 8\,\mathrm{M_\odot}$ (Verbunt & van den Heuvel (1994)). The main distinction between LMXBs and HMXBs is the mass of the optical companion with a broad, thinly populated dividing region between $\sim 1-5\,\mathrm{M_\odot}$. This difference results in drastically different evolution time-scales for low and high mass X-ray binaries and, hence, different relations of their number and collective luminosity to the instantaneous star formation activity and the stellar content of the parent galaxy. In the case of a HMXB, having a high mass companion, generally $M_{\mathrm{optical}} \gtrsim 10\,\mathrm{M_\odot}$ (Verbunt & van den Heuvel (1994)), the characteristic time-scale is at most the nuclear time-scale of the optical companion which does not exceed $\sim 2 \times 10^7$ years whereas for a LMXB, generally $M_{\mathrm{optical}} \lesssim 1\,\mathrm{M_\odot}$, it is of the order of $\sim 10^{10}$ years.

The CHANDRA X-ray observatory studied the distributions and luminosity functions of X-ray binaries in a number of nearby galaxies. These observations by CHANDRA have a great advantage compared to observations of X-ray sources in our Galaxy: All objects observed in a particular galaxy are equidistant and therefore it is straightforward to construct the luminosity function in the CHANDRA band. However, even with the sensitivity of CHANDRA we are

---

⋆ E-mail: `hgrimm@head-cfa.cfa.harvard.edu`

restricted to nearby galaxies ($d \lesssim 30$ Mpc) and we are able to observe only the high luminosity end of the luminosity function.

Observations of compact sources inside our Galaxy on the other hand open the unique possibility to construct a luminosity function in a much broader range of luminosities and moreover due to optical observations it is possible to distinguish different kinds of X-ray binaries in the Milky Way. However due to our location in the Galaxy, we need distance information for each individual system to reconstruct the luminosity distribution.

Using data from the all sky monitor (ASM) onboard RXTE, existing information about source distances and a model of the mass distribution in the Milky Way we were able to recover the spatial distribution and to construct the luminosity function of high and low mass X-ray binaries in our Galaxy. With this detailed knowledge about X-ray binaries in the Milky Way it is possible to compare them with X-ray binary populations in other galaxies observed by CHANDRA or XMM.

2 GALACTIC X-RAY BINARIES

2.1 Data

In order to construct the luminosity functions of Galactic X-ray binaries we used the publicly available data of ASM. The ASM instrument is sensitive in the 2–10 keV energy band which provides 80% sky coverage for every satellite orbit ($\sim$90 minutes). Due to its all-sky nature and long operational time, ~ 5 years, the ASM instrument is ideally suited for studying time averaged properties of sources. The light curves are obtained by RXTE GOF (Levine et al. (1996)) for a preselected set of sources from the ASM catalogue. A description of the catalogue and selection criteria can be found at Lochner & Remillard (1997). The ASM count rate has been converted to energy flux assuming a Crab-like spectrum.

The light curves have been averaged over the entire period of available data which might differ for different sources. We did not account in any way for orbital variations or eclipses, as e.g. in Cen X-3.

We selected X-ray binaries from the sample and divided them into low mass (LMXB) and high mass (HMXB) binaries according to the mass of the optical companion, using the mass of the secondary, M_2, of $2.5\,M_\odot$ to separate high and low mass systems. The precise value of this boundary affects classification of only few X-ray binaries (Her X-1, GX 1+4, GRO J1655–40 etc.). In doing so we used SIMBAD database, the Catalogue of X-ray Binaries (van Paradijs (1994)), the Catalogue of CV, LMXB and related objects (Ritter & Kolb (1998)), the catalogues of low-mass X-ray binaries (Liu et al. (2001)) and high-mass X-ray binaries (Liu et al. (2000)) and in some cases publications on individual sources.

In order to study the *spatial* distribution of X-ray binaries we collected source distances from the literature. We found distances for 140 X-ray binaries from the ASM sample. For X-ray binaries with an average flux above the ASM completeness limit used for constructing the luminosity functions, distances were determined for all but 8 sources. In cases when the published distance estimates disagree significantly we used the least model dependent estimates or their average.

2.2 Completeness

Important for the analysis presented below are two aspects of completeness:

1. completeness flux limit of the ASM sample of the X-ray sources
2. completeness of the sample of galactic X-ray binaries which are optically identified and for which distance measurements are available

In order to indirectly probe the completeness limit of the ASM sample we use the fact that the $\log(N) - \log(S)$ relation for extragalactic sources is well known and follows a power law with index $-3/2$ (Forman et al. (1978)), down to $\sim 3.8 \times 10^{-14}$ erg s^{-1} cm^{-2} (Ogasaka et al. (1998)) which corresponds to ASM count rate of 1.2×10^{-4} cnts s^{-1}. The $\log(N) - \log(S)$ relation for extragalactic sources based on ASM data is compared with HEAO A-1 and ASCA results. Flattening of the source counts caused by incompleteness of the sample begins at a count rate of ~ 0.1 cnts s^{-1}.

Therefore we set, somewhat arbitrarily, the completness limit of the ASM sample of the X-ray sources at 0.2 cnts s^{-1}. We verified that our conclusions are not sensitive to the exact value.

2.3 Spatial distribution

Despite the still relatively small number of X-ray sources and the sometimes poor accuracy of distance determinations it is now possible to compare the observed distribution of XRBs with theoretical expectations. Because of the flux limited nature of the ASM sample knowledge of the spatial distribution is required in order to derive the luminosity function. It is still not possible to unambiguously determine shape and parameters of the XRB distribution. We therefore adopted an approach in which we use the standard model of the stellar mass distribution in the Galaxy as a starting point and adjust, whenever possible, its parameters to fit observed distributions of low and high mass X-ray binaries. As the luminosity function depends somewhat on the assumed spatial distribution, we verify that variations of the parameters, which can not be determined from the data do not affect derived luminosity functions significantly.

The all-sky map shown in Fig.1 demonstrates how different the angular distributions of high and low mass X-ray binaries are over the sky. This fact is further illustrated by the angular distributions against Galactic latitude and longitude shown in Fig. 2. The figures illustrate the well-known fact that HMXBs are strongly concentrated towards the Galactic plane. In addition a strong difference in longitude distributions of HMXBs and LMXBs can be noticed, with the
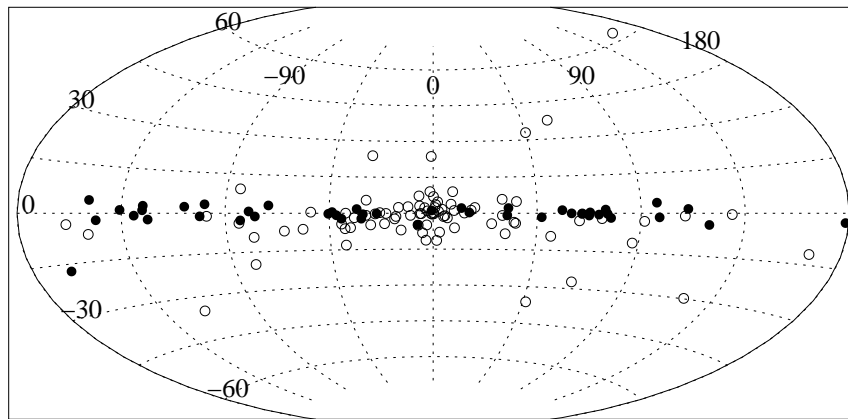
Fig. 1 Distribution of LMXBs (open circles) and HMXBs (filled circles) in the Galaxy. In total 86 LMXBs and 52 HMXBs are shown. Note the significant concentration of HMXBs towards the Galactic Plane and the clustering of LMXBs in the Galactic Bulge.
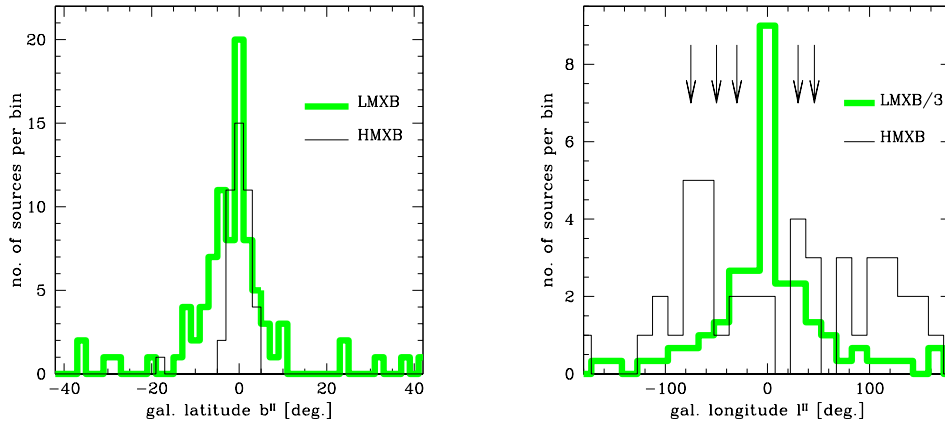
Fig. 2 Distribution of Galactic HMXBs (solid lines) and LMXBs (thick grey lines) against Galactic latitude b^{II} (left panel) and longitude l^{II} (right panel). The arrows in the right panel mark the positions of the tangential points of spiral arms. Note that on the right panel the number of LMXBs is divided by 3.

latter significantly concentrated towards the Galactic Centre/Bulge and the former distributed in clumps approximately coinciding with the location of tangential points of the spiral arms, see e.g. Englmaier & Gerhard (1999); Simonson (1976).

2.3.1 The Galaxy model

We employ the standard three component model of the stellar mass distribution in the Galaxy (Bahcall & Soneira (1980)), consisting of bulge, disk and spheroid. We also included a modification of the standard disk component taking into account spiral arms. Their description is based on the model of Georgelin & Georgelin (1976) in the implementation by Taylor & Cordes (1993). For details of the Galaxy model see Grimm et al. (2002).

All three components of the standard Galaxy model were used to construct the spatial distribution of LMXB. The spheroid component with appropriately adjusted normalisation was used to account for the population of globular cluster sources. Based on the observed distribution and theoretical expectation that HMXBs trace the star forming regions in the Galaxy, only the disk component was used for the spatial distribution of HMXBs.

2.3.2 High mass X-ray binaries

The angular distribution of HMXBs in Fig. 2 shows signatures of the Galactic spiral structure. These signatures are clearly seen in the distribution of sources over galactic longitude which shows maxima approximately consistent with directions towards tangential points of the spiral arms. No significant peak in the direction to the Galactic centre is present. In Fig. 4 the radial distribution of the smaller sample of sources for which distance measurements are available, shows pronounced peaks at the locations of the major spiral arms and is similar to that of primary tracers of the Galactic spiral structure – giant HII regions (e.g. Downes et al. (1980)) and warm molecular clouds (e.g. Solomon et al. (1985)). In particular, the central ~ 3–$4\,\mathrm{kpc}$
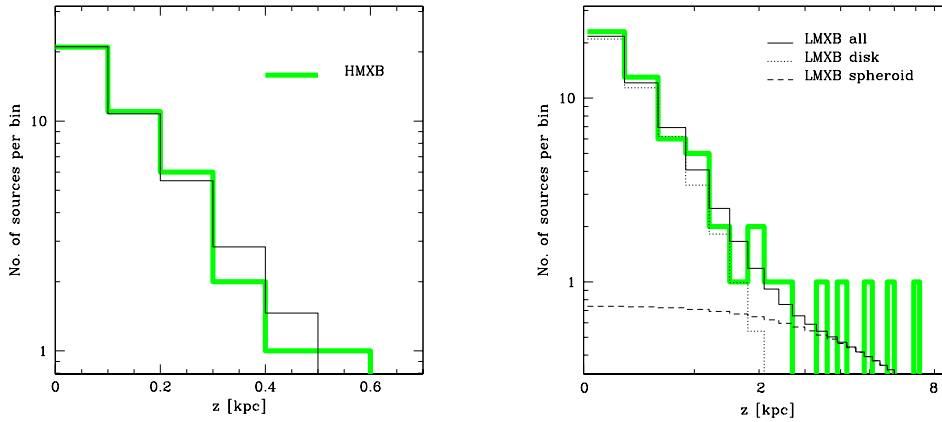
Fig. 3 Vertical distributions of high mass (left panel) and low mass (right panel) X-ray binaries. The vertical distributions were summed over northern and southern galactic hemispheres. In the case of LMXBs only sources with $R > 3.5$ kpc were used, to exclude bulge sources. Thick grey solid lines show the observed distributions and thin solid and dashed lines the expected distributions.
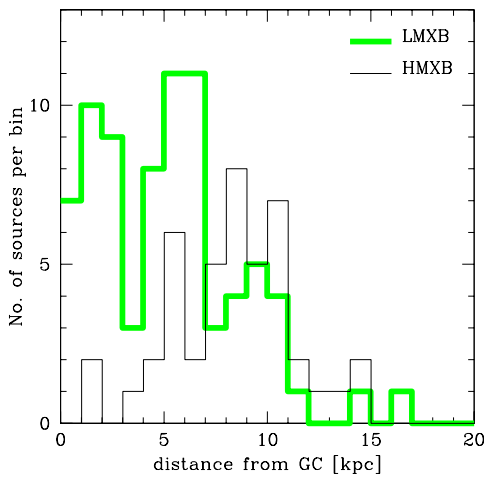
Fig. 4 Radial distributions of high mass (solid histogram) and low mass (thick grey histogram) X-ray binaries. The projected distance is defined as $\sqrt{x^2 + y^2}$, where x and y are Cartesian coordinates in the Galactic plane Note that the plotted distributions are not corrected for the volume of cylindrical shells ($\propto r$).

region of the Galaxy is almost void of HMXB well in accordance with the radial distribution of the giant HII regions and warm CO clouds.

The vertical distribution of HMXBs is significantly more concentrated towards the Galactic Plane and sufficiently well described by a simple exponential with a scale height of 150 pc as shown in the left panel of Fig. 3.

Based on theoretical expectations and on the data shown in Figs. 1, 2, 3 and 4, we included only the disk component in the volume density distribution of HMXBs. However a simple exponential disk is not a good description for the radial distribution of HMXB. Therefore, following Dehnen & Binney (1998) we assumed the disk density distribution to have three exponential terms, where the first term in the exponential allows for a central density depression.

The spiral arms were assumed to have a Gaussian density profile along the Galactic Plane. For details see Grimm et al. (2002).

2.3.3 Low mass X-ray binaries

Contrary to HMXB, the angular distribution of LMXBs is strongly peaked in direction to the Galactic centre and declines gradually along the Galactic plane, see Fig. 2. The central ~ 2 kpc region is densely populated with Galactic Bulge LMXB sources and contains $\sim 1/3$ of the LMXBs from our flux limited sample (Fig. 4). Similar to HMXBs, the signatures of the spiral structure might be present in the radial distribution although they are less pronounced.

The vertical distribution outside the bulge (Fig. 3) is significantly broader than that of HMXBs and includes a number of sources at high galactic z. The observed z-distributions cannot be adequately described by a simple exponential law. As only three out of nine sources at $|z| > 2$ kpc are located in globular clusters, this tail of high-z sources cannot be solely due to the globular cluster component. The relatively small number of high-z sources does not allow one to determine the shape of their distribution based on the data only. In order to account for the high-z sources and the LMXB sources in globular clusters we chose to include in the spatial distribution of LMXBs the spheroid component described by a de Vaucouleurs profile, that correctly represents the distribution of globular clusters. The overall vertical distribution can be adequately represented by a sum of an exponential law with a scale height of 410^{+100}_{-80} pc and a de Vaucouleurs profile with scale length of 2.8 kpc. The spheroid component represented by the de Vaucouleurs profile contains $\sim 25\%$ of the total number of LMXBs. Note, that this number is by a factor of ~ 2–3 larger than the mass fraction of the stellar spheroid in the standard Galaxy model. The enhanced fraction of the spheroid component is generally consistent with the fact, that the number of X-ray sources per unit mass is ~ 100 times higher in the globular clusters than in the Galactic disk and 12 out of 104 LMXBs in our sample are globular cluster sources.
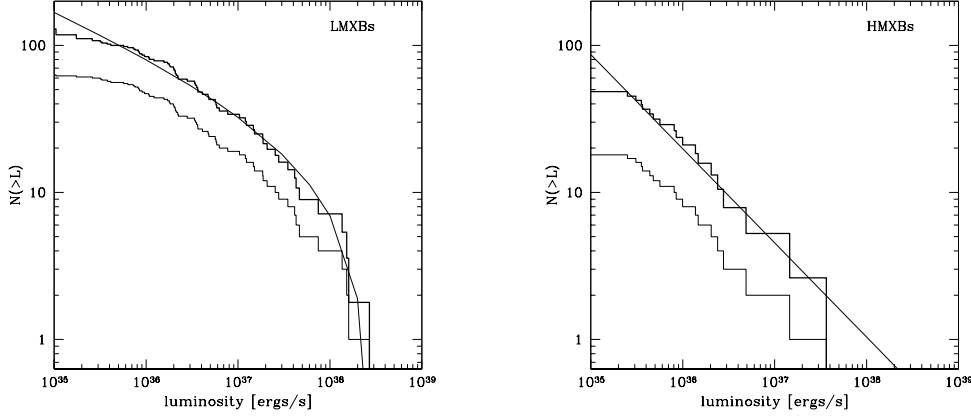
3 LUMINOSITY FUNCTION

Due to the flux limited nature of the ASM sample and incompleteness of the optical identifications/distance measurements beyond ~ 10 kpc, the *apparent* luminosity function which can be derived straightforwardly from the ASM flux measurements and the source distances (thin line histograms in Fig. 5) needs to be corrected for the fraction of the Galaxy observable by ASM. This correction can be performed using the model of the spatial distribution of X-ray binaries constructed in the previous section:

$$\frac{dN}{dL} = \left(\frac{dN}{dL}\right)_{\text{obs}} \times \frac{M(< D(L))}{M_{\text{tot}}} , \tag{1}$$

where $\frac{dN}{dL}$ is the true luminosity function, $\left(\frac{dN}{dL}\right)_{\text{obs}}$ – apparent luminosity function constructed using ASM flux measurements and the source distances, $M(< D)$ – mass of the Galaxy inside distance D from the Sun computed using the galaxy model with the corresponding parameters for LMXBs and HMXBs, respectively, M_{tot} – total mass of the Galaxy, $D(L)$ is defined by:

$$D(L) = \min\left(\frac{L}{\sqrt{4\pi F_{\text{lim}}}}, \ D_{\text{max}}\right) , \tag{2}$$

where F_{lim} is the limiting (minimum) flux and D_{max} – the maximum distance from the Sun of the sources used for constructing the luminosity function. As discussed in the previous sections we accepted the following selection criteria: $F_{\text{lim}} = 0.2$ cnts s$^{-1} \approx 6.4 \times 10^{-11}$ erg s^{-1} cm^{-2}, i.e.

Fig. 5 The apparent (thin histogram) and volume corrected (thick histogram) cumulative luminosity function for LMXBs and HMXBs. The solid lines are the best fits to the data.

equal to the completeness flux limit of the ASM catalogue, and $D_{\max} = 10\,\mathrm{kpc}$ – a completeness limit of distance measurements.

Obviously, for a given flux limit $F_{\lim}$ the mass fraction of the Galaxy $\frac{M(<D(L))}{M_{\mathrm{tot}}}$ is a decreasing function of the source luminosity. For the ASM sensitivity/completeness limit of $\approx 6.4 \times 10^{-11}$ erg s^{-1} cm^{-2} the entire volume inside $D_{\max} = 10$ kpc from the Sun is observable down to a luminosity of $\approx 10^{36}$ erg s^{-1} below which the mass fraction of the observable part of the Galaxy begins to decrease. As the spatial distributions of HMXB and LMXB sources differ significantly, the volume correction and the luminosity function were calculated separately for HMXBs and LMXBs. The volume corrected (true) cumulative luminosity functions are presented in Fig. 5.

The cumulative luminosity function of HMXBs (Fig. 5, right panel) does not seem to contradict to a power law distribution down to a luminosity of $\sim 2 \times 10^{35}$ erg s^{-1} with some indication of flattening at lower luminosity. We therefore fitted the luminosity function of HMXBs in the $L > 2 \times 10^{35}$ erg s^{-1} range with a power law distribution. Using a Maximum-Likelihood method the best fit parameters are:

$$N(> L) = 20 \times \left(\frac{L}{10^{36}\mathrm{erg\ s}^{-1}}\right)^{-0.64\pm0.15}, \tag{3}$$

where L is the source luminosity in erg s^{-1} and $N(> L)$ – total number of sources on the sky with luminosity greater than L.

The shape of the luminosity function for LMXBs (Fig. 5, left panel) indicates the presence of a high luminosity cut-off. We fitted the unbinned cumulative distribution with a functional form corresponding to a power law differential luminosity function with a sharp cut-off at $L_{\max}$. The value of the cutoff was set equal to to 2.7×10^{38} erg s^{-1} which corresponds to the luminosity of the most luminous source within 10 kpc, Sco X-1. The best fit values of other parameters are:

$$N(> L) = 105 \cdot \left(\left(\frac{L}{10^{36}\mathrm{erg\ s}^{-1}}\right)^{-0.26\pm0.08} - 270^{-0.26}\right). \tag{4}$$

Note that the smaller number of sources and the steeper slope of luminosity function make the HMXB data insensitive to a high luminosity cut-off above $\sim$ few $\times 10^{36}$ erg s^{-1}.

The integrated luminosity of HMXBs and LMXBs in the 2–10 keV ASM band are $\approx 2 \times 10^{38}$ erg s^{-1} and $\approx 2.5 \times 10^{39}$ erg s^{-1}, respectively. Note that these numbers refer to the luminosity *averaged* over the period from 1996–2000. The variability of individual sources or an outburst of a bright transient can change the luminosity by a factor of up to $\sim 2 - 3$. Due to the shallow slopes of the luminosity functions the integrated X-ray emission of the Milky Way is dominated by the $\sim 5 - 10$ most luminous sources.

3.1 Extension to low luminosities

In order to study the low flux regime below the ASM completeness limit of $\approx 6.4 \times 10^{-11}$ erg s^{-1} cm^{-2}, we use ASCA data from the Galactic Ridge Survey Sugizaki et al. (2001) covering ≈ 40 square degrees with the limiting sensitivity of $\sim 3 \times 10^{-13}$ erg s^{-1} cm^{-2}. For source selection we followed the criterion suggested by Sugizaki et al. (2001) in order to discriminate X-ray binary candidates from other sources. Excluding otherwise identified sources with these spectral properties there remain 28 sources.

Knowledge of the $\log(N) - \log(S)$ observed by ASCA and the spatial distribution of sources in the Galaxy gives a possibility to constrain the low luminosity end of the luminosity function. If the luminosity function observed with ASM continues to lower luminosities then it should be possible to reproduce the $\log(N) - \log(S)$ observed by ASCA according to the formula

$$N(> S) = \int_{L_{\min}}^{L_{\max}} \frac{dN}{dL} \times \frac{M(< r)_{\text{ASCA}}}{M_{\text{total}}} dL, \ \text{with} \ r = \sqrt{\frac{L}{4\pi \cdot S}} \ . \tag{5}$$

where $N(> S)$ is the number of sources with a flux higher than S observed by ASCA, $\frac{dN}{dL}$ is the differential luminosity function, and $\frac{M(<r)_{\text{ASCA}}}{M_{\text{total}}}$ is the fraction of mass within a radius r from the Earth within the field of view of the ASCA survey, $L_{\max}$ is the high luminosity cut-off of the luminosity function (Eqs. (3) and (4)). $L_{\min}$ is the low luminosity cut-off of the luminosity function below which it is assumed to be equal to zero. This quantity characterises roughly the luminosity level at which the luminosity function deviates significantly from the extrapolation of the ASM power law.

The predicted $\log(N) - \log(S)$ calculated from Eq. (5) is compared with the $\log(N) - \log(S)$ of X-ray binary candidates from the ASCA survey in Fig. 6. The predicted $\log(N) - \log(S)$ was calculated according to Eq. (5) separately for HMXB and LMXB using the extrapolation of the respective ASM luminosity functions. The mass integral $M(< r)$ in Eq. (5) was calculated taking approximately into account the actual pattern of ASCA pointings and using the volume density distributions of our galaxy model.

It is clear from Fig. 6 that the predicted number–flux relation of X-ray binaries agrees with the ASCA data very well. The good agreement with the predicted $\log(N) - \log(S)$ distribution implies that the data do not require a low luminosity cut-off of the luminosity function down to $\sim 10^{34}$ erg s^{-1}.

4 CONNECTION BETWEEN HMXBS AND STAR FORMATION RATE

4.1 Sample

Our sample of galaxies is tripartite, first, galaxies whose X-ray binary population has been spatially resolved by CHANDRA, second galaxies that have no XRB luminosity function, but
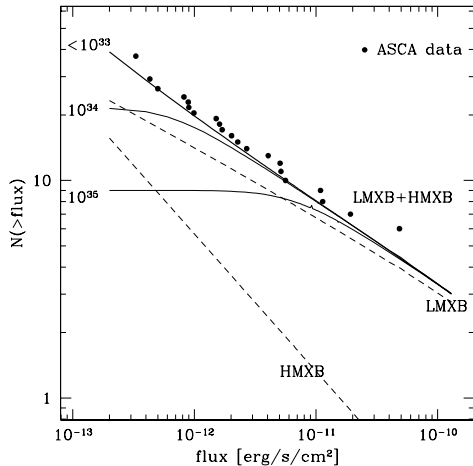
Fig. 6 Comparison of the $\log(N) - \log(S)$ observed in the ASCA Galactic Ridge Survey (points) and the predicted $\log(N) - \log(S)$ based on the extrapolation of the ASM luminosity function to low luminosities (lines), according to Eq. (5). The vertical axis shows the number of sources in the entire field of the ASCA survey. We added five bright sources located in the ASCA field of view that were excluded from the final catalogue in Sugizaki et al. (2001) and corrected for the flux dependent sky coverage (Fig. 7 in Sugizaki et al. (2001)). Thick solid lines – combined $\log(N) - \log(S)$ of LMXBs and HMXBs for different values of L_{min}, thin dashed lines – contributions of LMXBs and HMXBs separately for the case without cut-off.

for which X-ray flux measurements are available (mainly from ASCA), and, third, galaxies at high redshift($z \sim 0.2$–1.3), mostly in the Hubble Deep Field-North. We ensured that the SFR of these galaxies was high enough that HMXBs should dominate over LMXBs by comparing their SFR estimates with mass estimates, only for the high-z sample this was not possible for all galaxies. Moreover the second and third part of the sample was restricted to galaxies that do not exhibit AGN-related activity.

In order to probe the HMXB luminosity function in the low SFR regime, we used the results of the X-ray binary population study in the Milky Way by Grimm et al. (2002), based on RXTE/ASM observations and the luminosity function of high mass X-ray binaries in the Small Magellanic Cloud obtained by ASCA Yokogawa et al. (2000).

To estimate X-ray luminosity and star formation rate and compare these values for different galaxies it is necessary to have a consistent set of distances. The distances were calculated using velocities from Sandage & Tammann (1980) corrected to the centre of mass of the Local Group and assuming a Hubble constant value of $H_0 = 70$ km s^{-1} Mpc^{-1}. Note that these distances might differ from the values used in the original publications on the X-ray luminosity functions and SFRs.

One of the most serious issues important for the following analysis is the completeness level of the luminosity functions which is obviously different for different galaxies, due to different exposure times and distances. In those cases when the completeness luminosity was not given in the original publication, we used a conservative estimate based on the luminosity at which the luminosity function starts to flatten.

One of the main uncertainties involved is related to the SFR estimates. Conventional SFR indicators rely on a number of assumptions regarding the environment in a galaxy, such as dust content of the galaxy, or the shape of the initial mass function (IMF). In order to roughly assess the amplitude of the uncertainties in the SFR estimates we compared results of different star formation indicators for each galaxy from our sample with special attention given to the galaxies from the primary sample. In order to convert the flux measurements to star formation rates we use the result of an empirical cross calibration of star formation rate indicators by Rosa-González et al. (2002). The calibration is based on the canonical formulae by Kennicutt (1998) and takes into account dust/extinction effects. The term SFR refers to the star formation rate of stars more massive than ~ 5 M$_\odot$.
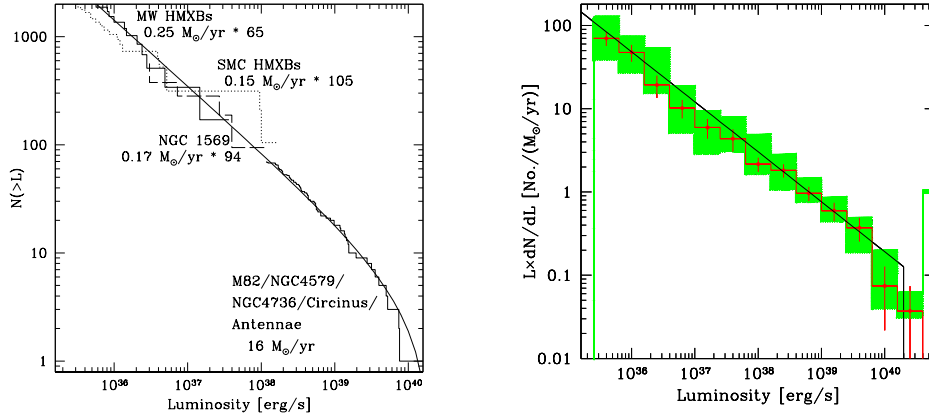
Fig. 7 *Left:* Combined luminosity function of compact X-ray sources in the starburst galaxies M82, NGC 4038/9, NGC 4579, NGC 4736 and Circinus ($L > 2 \times 10^{38}$ erg s^{-1}) and the luminosity functions of NGC 1569 and HMXBs in the Milky Way and SMC. The thin solid line is the best fit to the combined luminosity function of the starburst galaxies *only*, given by Eq. 7. *Right:* Differential luminosity function obtained by combining the data for *all* galaxies from the primary sample, except for NGC 3256. The straight line is the best fit to the luminosity function of star forming galaxies given by Eq. 6. The grey area is the 90 per cent confidence level interval we obtained from a Monte-Carlo simulation taking into account uncertainties in the SFR and distances.

For a detailed discussion of the sample and the derivations of its properties refer to Grimm et al. (2003).

4.2 Universal Luminosity function

In order to obtain the universal luminosity function of HMXBs we fit the combined luminosity function of M 82, Antennae, NGC 4579, NGC 4736 and Circinus using a Maximum-Likelihood method with a power law with a cut-off at $L_c = 2.1 \times 10^{40}$ erg s^{-1} and normalise the result to the combined SFR of the galaxies. The best fit luminosity function (solid line in Fig.7) in the differential form is given by:

$$\frac{dN}{dL_{38}} = (3.3^{+1.1}_{-0.8}) \cdot \text{SFR} \cdot L_{38}^{-1.61 \pm 0.12} \quad \text{for } L < L_c, \tag{6}$$

where $L_{38} = L/10^{38}$ erg s^{-1} and SFR is measured in units of M$_\odot$ yr^{-1}. The errors are 1σ estimates for one parameter of interest. The rather large errors for normalisation are due to the correlation between slope and normalisation of the luminosity function, with a higher value of normalisation corresponding to a steeper slope. The cumulative form of the luminosity function, corresponding to the best values of the slope and normalisation is:

$$N(> L) = 5.4 \cdot \text{SFR} \cdot (L_{38}^{-0.61} - 210^{-0.61}), \tag{7}$$

According to a Kolmogorov-Smirnov test the data are consistent with the best fit model at a confidence level of 90 per cent.
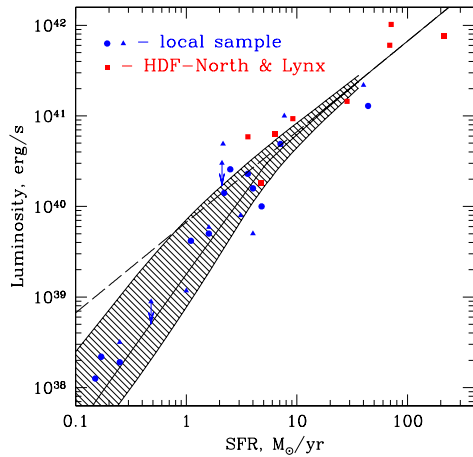
Fig. 8 The L_X-SFR relation. The filled circles and triangles are nearby galaxies and, the open circles are distant star forming galaxies from the HDF North and Lynx field. The arrows are upper limits for the X-ray luminosity due to HMXBs for IC 342 and NGC 891. The thick solid line shows the expected relation between SFR and the most probable value of the total luminosity computed for the best fit parameters of the HMXB luminosity function (exact calculation, from Gilfanov et al. (2003)). The shaded area shows the 68 per cent confidence region including both intrinsic variance of the L_X–SFR relation and uncertainty of the best fit parameters of the HMXB luminosity function (Eq. (6)). The dashed line shows the linear L_X–SFR relation given by Eq. (9).

4.3 Total X-ray luminosity as SFR indicator

CHANDRA and future X-ray missions with angular resolution of the order of $\sim 1''$ would be able to spatially resolve X-ray binaries only in nearby galaxies ($d \lesssim \sim 50\,\mathrm{Mpc}$). For more distant galaxies only the total luminosity of a galaxy due to HMXBs can be used for X-ray diagnostics of star formation.

Figure 8 shows the total luminosity of X-ray binaries (above 10^{36} erg s^{-1}) plotted versus SFR. The galaxies spatially resolved by CHANDRA are shown by filled circles. The galaxies, for which only total luminosity is available are shown as filled triangles. The luminosities of the galaxies were either calculated by summing the luminosities of individual sources down to the completeness limit of the corresponding luminosity function, the contribution of the sources below the completeness limit was approximately accounted for by integrating a power law distribution with slope 1.6 and normalisation obtained from the fit to the observed luminosity function, or by directly converting the measured flux to luminosity. The total luminosity depends only weakly on the lower integration limit.

Interestingly the relation is composed of two parts, a non-linear part at low SFR and a linear at high SFR. This behaviour is due to the statistical properties of a power law distribution. For details see Gilfanov et al. (2003). The X-ray luminosity scales asymptotically in the non-linear part as

$$L_X = 2.6 \times 10^{39} \cdot \mathrm{SFR}^{1.7} [M_\odot \mathrm{yr}^{-1}] \tag{8}$$

and in the linear regime as

$$L_X = 6.7 \times 10^{39} \cdot \mathrm{SFR} [M_\odot\,\mathrm{yr}^{-1}]. \tag{9}$$

The solid line in Fig.8 shows the result of the exact calculation of the L_X–SFR relation from Gilfanov et al. (2003). The relation was computed for the best fit parameters of the HMXB luminosity function determined from the analysis of five mostly well studied galaxies from the CHANDRA observed sample.

Figure 8 demonstrates sufficiently good agreement between the data and the theoretical L_X–SFR relation. Importantly, the predicted relation agrees with the data both in the high and low SFR regime, thus showing that the data, including the high redshift galaxies from Hubble

Deep Field North, are consistent with the HMXB luminosity function parameters, derived from significantly fewer galaxies than plotted in Fig. 8.

The existence of the linear part at SFR $>$5–10 M$_\odot$ yr^{-1} gives an independent confirmation of the reality of the cut-off in the luminosity function of HMXBs. The position of the break and normalisation of the linear part in the L_X-SFR relation confirms that the maximum luminosity of the HMXB sources (cut-off in the HMXB luminosity function) is of the order of $L_c \sim 10^{40}-10^{41}$ erg s^{-1} (see Gilfanov et al. (2003) for more details). Despite the number of theoretical ideas being discussed, the exact reason for the cut-off in the HMXB luminosity function is not clear and significant variations of L_c among galaxies, related or not to the galactic parameters, such as metalicity or star formation rate can not be excluded a priori. However, significant variations in L_c from galaxy to galaxy would result in large dispersion in the break position and in the linear part of the L_X-SFR relation. As such large dispersion is not observed, one might conclude that there is no large variation of the cut-off luminosity between galaxies and, in particular, there is no strong dependence of the cut-off luminosity on SFR.

References

Bahcall, J. N. & Soneira, R. M. 1980, ApJS, 44, 73

Dehnen, W. & Binney, J. 1998, MNRAS, 294, 429

Downes, D., Wilson, T. L., Bieging, J., & Wink, J. 1980, A&AS, 40, 379

Englmaier, P. & Gerhard, O. 1999, MNRAS, 304, 512

Fabbiano, G. 1994, Cambridge Astrophysics Series, Vol. 26, X-ray binaries (Cambridge University Press), 390

Forman, W., Jones, C., Cominsky, L., et al. 1978, ApJS, 38, 357

Georgelin, Y. & Georgelin, Y. 1976, A&A, 49, 57

Gilfanov, M., Grimm, H.-J., & Sunyaev, R. 2003, in preparation

Grimm, H.-J., Gilfanov, M., & Sunyaev, R. 2002, A&A, 391, 923

Grimm, H.-J., M., G., & R., S. 2003, MNRAS, 339, 793

Kennicutt, R. C. 1998, ARA&A, 36, 189

Levine, A. M., Bradt, H., Cui, W., et al. 1996, ApJ, 469, L33

Liu, Q. Z., van Paradijs, J., & van den Heuvel, E. P. J. 2000, A&AS, 147, 25

Liu, Q. Z., van Paradijs, J., & van den Heuvel, E. P. J. 2001, A&A, 368, 1021

Lochner, J. & Remillard, R. 1997, The XTE All Sky Monitor Data Products, http: // heasarc. gsfc. nasa.gov/ docs/ xte/ asm_products_guide.html

Ogasaka, Y., Kii, T., Ueda, Y., et al. 1998, AN, 319, 43

Ritter, H. & Kolb, U. 1998, A&AS, 129, 83

Rosa-González, D., Terlevich, E., & Terlevich, R. 2002, MNRAS, 332, 283

Sandage, A. & Tammann, G. A. 1980, A revised Shapley-Ames Catalog of bright galaxies (Washington: Carnegie Institution, 1980, Preliminary version)

Simonson, S. C. 1976, A&A, 46, 261

Solomon, P., Sanders, D., & Rivolo, A. 1985, ApJL, 292, 19

Sugizaki, M., Mitsude, K., Kaneda, H., et al. 2001, ApJS, 134, 77

Taylor, J. & Cordes, J. 1993, ApJ, 411, 674

van Paradijs, J. 1994, Cambridge Astrophysics Series, Vol. 26, X-ray binaries (Cambridge University Press), 536

Verbunt, F. & van den Heuvel, E. 1994, Cambridge Astrophysics Series, Vol. 26, X-ray binaries (Cambridge University Press), 457

Yokogawa, J., Kensuke Imanishi, M. T., Nishiuchi, M., & Koyama, K. 2000, ApJS, 128, 491

DISCUSSION

K. WU: How do the uncertainties of the host galaxies affect the uncertainties of the luminosity function, in particular in the uncertainty in the luminosity axis? Do they affect the high L break at 10^{40} erg s^{-1}?

H.-J. GRIMM: The uncertainties affect the luminosity axis only insofar as the distances of individual galaxies change. Therefore we used a consistent set of distances to minimize this problem. This change in individual distances would dilute the cut-off, and this gives rise to an uncertainty in the existence of the cut-off. However, the HDF data and very high SFR galaxies lie on a linear part of the L_X-SFR relation. thereofre this is an independent confirmation of the existence of a cut-off, even if we can only say for now that it is around 10^{40}–10^{41} erg s^{-1}.

J. BECKMAN: How did you calibrate your SFRs given the uncertainties you mentioned in your discussion? Also how dependent is the SFR you use on the IMF of the stellar population?

H.-J. GRIMM: We minimized the uncertainties in SFR measurements by employing a range of different SFR indicators, UV, FIR, radio and H$_\alpha$. For most galaxies we have at least three different measurements of at least some of these indicators. We discarded the most deviation measurements if there were any and averaged the rest. The SFR is not very sensitive to the IMF since we restrict ourselves to SFRs for stars with more than 5 solar masses, and for these stars the different IMFs are rather similar.

F. VERBUNT: Most stars in the galaxies are transient. How do you handle the transients?

H.-J. GRIMM: We use the same procedure as for persistent sources. We averaged the flux over the time they were observed by ASM. This might lead to differences in the luminosity functions, considering that CHANDRA does snapshots and the Galactic luminosity functions are averaged over roughly 5 years. However two CHANDRA observations of Cen A that were a few months apart and even covered somewhat different parts of the galaxy do not show big changes in the luminosity function.